2.1 RAMAN LIDAR PROFILING OF WATER VAPOR AND AEROSOLS OVER THE ARM SGP SITE

Richard A. Ferrare[*1], David D. Turner[2], Lorraine A. Heilman[3], Wayne F. Feltz[4], Randy A. Peppler[5], Tim Tooman[6], Rangasayi Halthore[7]

[1]NASA Langley Research Center
[2]Pacific Northwest National Laboratory
[3]SAIC/NASA Langley Research Center
[4]University of Wisconsin-Madison
[5]University of Oklahoma
[6]Sandia National Laboratories
[7]Brookhaven National Laboratory

1. INTRODUCTION

We have developed and implemented automated algorithms to retrieve profiles of water vapor mixing ratio, aerosol backscattering, and aerosol extinction from Southern Great Plains (SGP) Cloud and Radiation Testbed (CART) Raman Lidar data acquired during both daytime and nighttime operations. This Raman lidar system is unique in that it is turnkey, automated system designed for unattended, around-the-clock profiling of water vapor and aerosols (Goldsmith et al., 1998). These Raman lidar profiles are important for determining the clear-sky radiative flux, as well as for validating the retrieval algorithms associated with satellite sensors. Accurate, high spatial and temporal resolution profiles of water vapor are also required for assimilation into mesoscale models to improve weather forecasts.

We have also developed and implemented routines to simultaneously retrieve profiles of relative humidity. These routines utilize the water vapor mixing ratio profiles derived from the Raman lidar measurements together with temperature profiles derived from a physical retrieval algorithm that uses data from a collocated Atmospheric Emitted Radiance Interferometer (AERI) and the Geostationary Operational Environmental Satellite (GOES) (Feltz et al., 1998; Turner et al., 1999). These aerosol and water vapor profiles (Raman lidar) and temperature profiles (AERI+GOES) have been combined into a single product that takes advantage of both active and passive remote sensors to characterize the clear sky atmospheric state above the CART site.

2. INSTRUMENTATION

The CART Raman Lidar (CARL) uses a tripled Nd:YAG laser, operating at 30 Hz with 400 millijoule pulses to transmit light at 355 nm. A 61-cm diameter telescope collects the light backscattered by molecules and aerosols at the laser wavelength and the Raman scattered light from water vapor (408 nm) and nitrogen (387 nm) molecules. These signals are detected by photomultiplier tubes and recorded using photon counting with a vertical resolution of 39 meters. A beam expander reduces the laser beam divergence to 0.1 mrad, thereby permitting the use of a narrow (0.3 mrad) as well as a wide (2 mrad) field of view. The narrow field of view, coupled with the use of narrowband (~0.4 nm bandpass) filters, reduces the background skylight and, therefore, increases the maximum range of the aerosol and water vapor profiles measured during daytime operations.

Water vapor mixing ratio profiles are computed using the ratio of the Raman water vapor signal to the Raman nitrogen signal. Relative humidity profiles are computed using these water vapor mixing ratio profiles and the temperature profiles from the AERI+GOES temperature retrievals. The water vapor mixing ratio profiles are integrated with altitude to derive precipitable water vapor (PWV). The CARL water vapor mixing ratio profiles and PWV retrievals are calibrated using the coincident nighttime measurements of precipitable water vapor (PWV) from the microwave radiometer (MWR) (Turner and Goldsmith, 1999). The CARL water vapor calibration factor derived in this manner over a period of 9 months has a standard deviation of approximately 4% (Turner et al., 1999).

The lidar water vapor mixing ratio profiles were compared with water vapor profiles measured by radiosondes equipped with Vaisala RS-80 H-humicap sensors. Figure 1a shows the mean bias and rms error between the CARL and radiosonde water vapor profiles. The radiosonde profiles are drier than the CARL profiles by about 10-15% during the day and about 5% during the night (Turner et al., 1999). Figure 1b shows that scaling the radiosonde water vapor profile, such that the radiosonde PWV matches the MWR PWV, reduces the differences between the CARL and radiosonde water vapor profiles to generally less than 5% and reduces the differences between measured and modeled longwave radiances (Turner et al., 1998).

[*]Corresponding author address: Richard Ferrare, Mail Stop 401A, NASA Langley Research Center, Hampton, Virginia 23681,
e-mail: r.ferrare@larc.nasa.gov

In *Symposium on Lidar Atmospheric Monitoring, 80th AMS Annual Meeting, Long Beach, January 9-14*, pp. 1-4, American Meteorological Society, 2000.

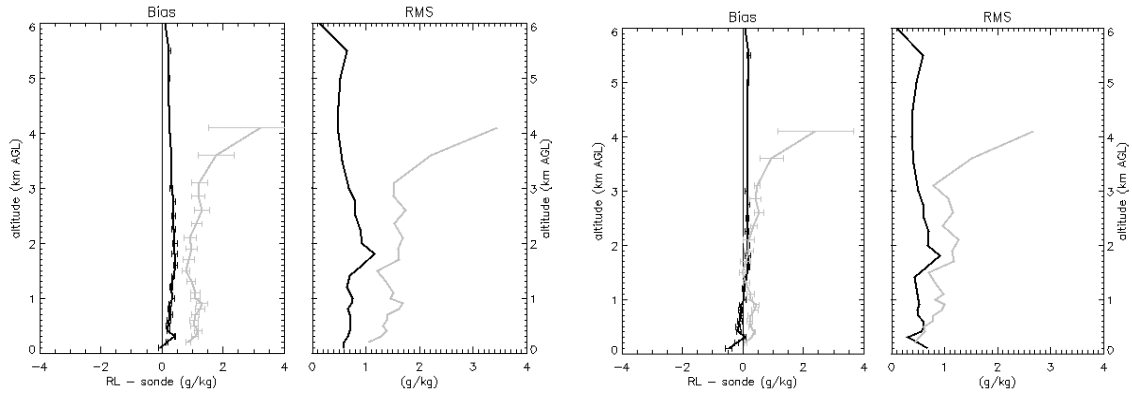

Figure 1a (left) Bias and rms differences between CARL and radiosonde water vapor mixing ratio profiles acquired during daytime (black) and daytime (grey) observations from April through December, 1998. 1b. (right) Same except that the radiosonde profiles were scaled to match the MWR PWV (from Turner et al., 1999).

Profiles of aerosol scattering ratio, which is the ratio of aerosol+molecular scattering to molecular scattering, are derived using the Raman nitrogen signal and the signal detected at the laser wavelength. Aerosol volume backscattering cross section profiles are then computed using the aerosol scattering ratio and molecular scattering cross section profiles derived from atmospheric density data. These density profiles are computed using coincident pressure and temperature profiles derived from radiances measured by the ground based AERI instrument and by the GOES satellite. Aerosol extinction cross section profiles are computed from the derivative of the logarithm of the Raman nitrogen signal with respect to range. The aerosol backscattering and extinction profiles derived in this manner are then used to measure profiles of the aerosol extinction/backscattering ratio. Aerosol optical thicknesses are derived by integration of the aerosol extinction profiles with altitude. Ferrare et al. (1998) provide additional information regarding these methods.

3. MEASUREMENTS

In this presentation, we discuss aerosol extinction, water vapor, and relative humidity profiles computed using the automated algorithms for Raman lidar data acquired between April 1, 1998 and April 30, 1999. During this period, CARL operated nearly 50% of the time, with electrical power interruptions responsible for most of the down time. A special un-interruptable power supply, which was installed for CARL during February 1999, should significantly reduce the power interruptions.

The high resolution Raman lidar water vapor measurements and AERI temperature measurements provide a much more detailed representation of the atmospheric state than can be achieved using radiosondes alone. These measurements depict in great detail the rapid atmospheric changes associated with the passages of dry lines and cold fronts over the SGP site. Figure 2 shows water vapor mixing ratio,

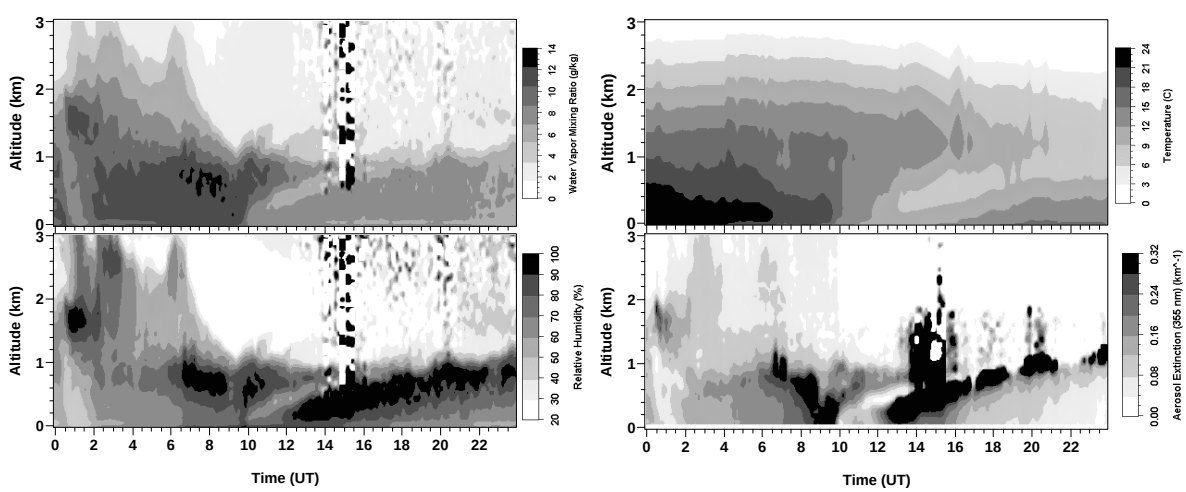

Figure 2. Profiles of water vapor mixing ratio (top left), relative humidity (bottom left), temperature (top right), and aerosol extinction (bottom right) measured over the SGP site on April 15, 1998 showing the passage of a cold front. Water vapor mixing ratio and aerosol extinction were derived from CARL, temperature from AERI, and relative humidity from both sensors. The vertical stripes that appear in the water vapor, relative humidity, and aerosol extinction images between 1400 and 1600 UTC are due to clouds.

relative humidity, temperature, and aerosol extinction profiles derived from CARL and AERI data acquired on April 15, 1998. These images show the passage of a cold front between 0900 and 1100 UTC. Note the rapid decrease in water vapor mixing ratio and temperature after the front passed over the site. An increase in aerosol extinction associated with hygroscopic aerosol growth can be seen between 0800 and 1000 UTC just prior to the frontal passage when the relative humidity increased above 70%. Turner et al. (1999) give a more complete description of this event and how the CARL and AERI data complement each other in characterizing the atmospheric state.

We have begun using the CARL aerosol data to characterize aerosol extinction, backscattering, and optical thickness over the SGP site. Aerosol optical thicknesses (AOT) were computed by integrating the Raman lidar aerosol extinction profiles between the

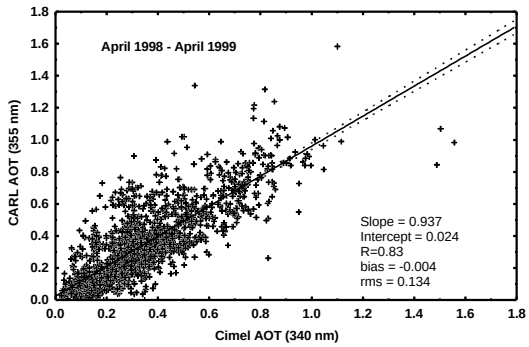

Figure 3. Comparison of AOT between Cimel sun photometer (340 nm) and Raman lidar (355 nm).

surface and 7 km. Figure 3 shows a comparison of the CARL AOT with simultaneous measurements of AOT acquired by a Cimel Sun photometer. The average bias difference between the CARL and Sun photometer AOT values was less than 5%.

Average aerosol extinction profiles were computed as a function of optical thickness to characterize the vertical distribution of aerosols. Figure 4 shows the distribution of AOT measured by CARL. Figure 5 shows

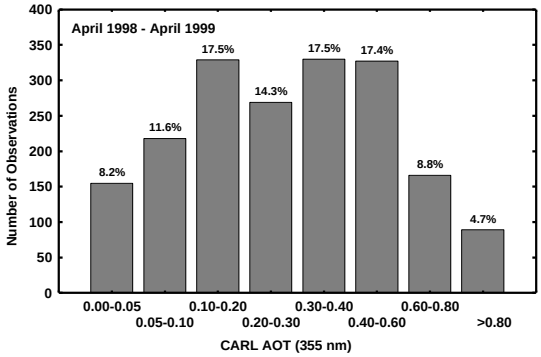

Figure 4. Distribution of AOT measured by CARL.

the average aerosol extinction profiles as a function of AOT. These profiles show the occurrence of high aerosol extinction values at altitudes of 3-6 km above the surface. In particular, aerosol extinction profiles acquired during May and August-September 1998 show episodes when high aerosol extinction was measured throughout several kilometers in the lower troposphere over several days. The Raman lidar aerosol extinction profiles derived during May 13-21 were most likely associated with the smoke from fires in Central America since observations by several satellite sensors and trajectory analyses indicated that smoke produced by these fires traveled over northern Oklahoma (Peppler et al., 1999). Profiles from this event display large variability in the both the magnitude and vertical distribution of aerosol extinction during these periods.

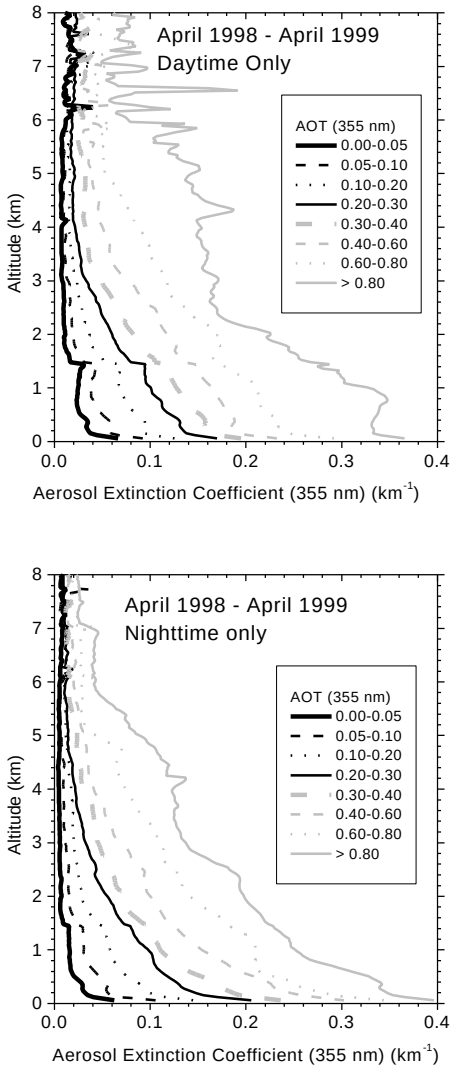

Figure 5. Average aerosol extinction profiles derived from daytime (top) and nighttime (bottom) CARL measurements.

We have also begun using these lidar aerosol and water vapor profiles to investigate lidar aerosol extinction/backscattering ratio (S_a), and the relationships among water vapor mixing ratio, relative humidity, aerosol extinction, and aerosol extinction/backscatter ratio for hygroscopic aerosols. CARL data often show that the aerosol extinction increased significantly when the relative humidity increased above 60-70% near the top of the boundary layer. Initial analyses also show that the aerosol extinction/backscattering ratio often increased with relative humidity in these cases. Figure 6 shows that the median value of S_a, which was computed using data through the entire period, increased with relative humidity in a manner somewhat similar to that represented by Ackerman (1998) for continental aerosols.

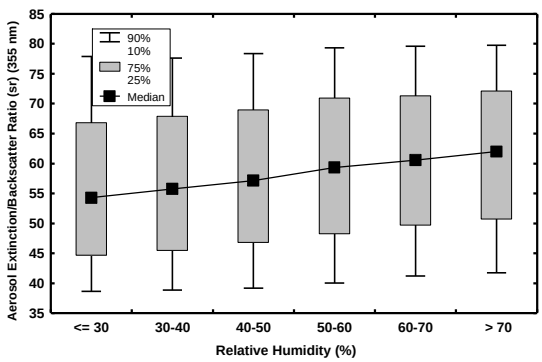

Figure 6. Distribution of the lidar aerosol extinction/backscatter ratio with relative humidity for data acquired between April 1998 and April 1999. Nighttime data below 8 km and daytime data below 3 km were used for this figure.

4. Summary

We have implemented algorithms to compute aerosol extinction and relative humidity profiles using CART Raman lidar data and AERI+GOES temperature retrievals. Together with Raman lidar water vapor mixing ratio, cloud mask, and depolarization retrievals, these aerosol and relative humidity profiles form a suite of products that are retrieved using automated remote sensing instruments and can be used to characterize the clear sky state over the SGP site. We are using these Raman lidar aerosol and water vapor measurements to investigate the relationships among water vapor and aerosols.

5. Acknowledgements

SGP CART Raman lidar, Cimel Sun photometer, and AERI data were obtained from the Atmospheric Radiation Measurement (ARM) Program sponsored by the U.S. Department of Energy, Office of Energy Research, Office of Health and Environmental Research, Environmental Sciences Division. The Cimel Sun photometer is also part of AERONET, a network of Sun photometers managed by B. N. Holben, NASA/GSFC. Funding for this work was provided by the NASA EOS Validation and DOE ARM Programs.

6. References

Ackerman, J., 1998: The Extinction-to-Backscatter Ratio of Tropospheric Aerosol: A Numerical Study, *J. Atmos. Oceanic Tech.,* **15**,1043-1050.

Feltz, W.F., W.L. Smith, R.O. Knuteson, H.E. Revercomb, H.M. Woolf, and H.B. Howell, 1998: Meteorological applications of temperature and water vapor retrievals from the ground-based atmospheric emitted radiance interferometer (AERI). *J. Appl. Meteor.,* **37**, 857-875.

Ferrare, R.A., S.H. Melfi, D.N. Whiteman, K.D. Evans, and R. Leifer, 1998: Raman lidar measurements of aerosol extinction and backscattering: Methods and comparisons. *J. Geophys Res*, **103**, 19663-19672.

Goldsmith, J.E.M., F.H. Blair, S.E. Bisson, and D.D. Turner, 1998: Turn-key Raman lidar for profiling atmospheric water vapor, clouds, and aerosols. *Appl. Opt*, **37**, 4979-4990.

Peppler, R.A., L. Ashford, C.P. Bahrmann, J.C. Barnard, R.A. Ferrare, R.N. Halthore, N.S. Laulainen, F.J. Murcray, J.A. Ogren, M.R. Poellot, P. Sheridan, M.E. Splitt, and D.D. Turner, 1999: Identification and analysis of the 1998 Central American smoke event at the ARM SGP Cart site. *Proceedings of the 9th ARM Science Team Meeting,* 23-25 March 1999, San Antonio, TX. http://www.arm.gov/docs/documents/technical/conf_9903/peppler-99.pdf

Turner, D.D., T.R. Shippert, P.D. Brown, S.A. Clough, R.O. Knuteson, H.E. Revercomb, and W.L. Smith, 1998: Long-term analysis of observed and line-by-line calculations of longwave surface spectral radiance and the effect of scaling the water vapor profile. *Proc 8th Atmospheric Radiation Measurement (ARM) Science Team Meeting*, Tuscon, AZ, 773-776. http://www.arm.gov/docs/documents/technical/conf_9803/turner-98.pdf.

Turner, D.D., and J.E.M. Goldsmith, 1999: 24-Hour Raman lidar measurements during the Atmospheric Radiation Measurement program's 1996 and 1997 water vapor intensive observation periods. *J. Atmos. Oceanic Technol.,* **16**, 1062-1076.

Turner, D.D., W.F. Feltz, R.A. Ferrare, 1999: Continuous water profiles from operational ground-based active and passive remote sensors, submitted to *Bull. Amer. Meteor. Soc.*